RESEARCH ARTICLE

Assessing the accuracy of georeferenced landcover data derived from oblique imagery using machine learning

James Tricker[1] (iD), Claire Wright[1], Spencer Rose[1], Jeanine Rhemtulla[2], Trevor Lantz[1] & Eric Higgs[1]

[1]School of Environmental Studies, University of Victoria, 3800 Finnerty Road, Victoria V8W 2Y2, British Columbia, Canada
[2]Department of Forest and Conservation Sciences, University of British Columbia, 2424 Main Mall, Vancouver V6T 1Z4, British Columbia, Canada

Abstract

Repeat photography offers distinctive insights into ecological change, with ground-based oblique photographs often predating early aerial images by decades. However, the oblique angle of the photographs presents challenges for extracting and analyzing ecological information using traditional remote sensing approaches. Several innovative methods have been developed for analyzing repeat photographs, but none offer a comprehensive end-to-end workflow incorporating image classification and georeferencing to produce quantifiable landcover data. In this paper, we provide an overview of two new tools, an automated deep learning classifier and intuitive georeferencing tool, and describe how they are used to derive landcover data from 19 images associated with the Mountain Legacy Project, a research team that works with the world's largest collection of systematic high-resolution historic mountain photographs. We then combined these data to produce a contemporary landcover map for a study area in Jasper National Park, Canada. We assessed georeferencing accuracy by calculating the root-mean-square error and mean displacement for a subset of the images, which was 4.6 and 3.7 m, respectively. Overall classification accuracy of the landcover map produced from oblique images was 68%, which was comparable to landcover data produced from aerial imagery using a conventional classification method. The new workflow advances the use of repeat photographs for yielding quantitative landcover data. It has several advantages over existing methods including the ability to produce quick and consistent image classifications with little human input, and accurately georeference and combine these data to generate landcover maps for large areas.

INTRODUCTION

Historical ground-based (i.e., oblique) landscape photographs are often overlooked as a source of information for studying ecological change (Keane et al., 2009; Trant et al., 2015; Webb et al., 2010). These photographs vary in coverage and quality, from snapshots in personal albums to extensive and systematic collections of images used for land surveying. What many early landscape photographs have in common is they serve as a record of ecosystems in most cases before the effects of pervasive human impacts (see Steffen et al., 2015). Oblique landscape photographs can provide researchers with a spatially explicit reference from which to evaluate contemporary landscape features and change, including, for example, species composition and configuration (Gruell, 1983; Hayward et al., 2012).

Methods for analyzing ecological change using historical oblique photographs were pioneered in the field of repeat photography: the practice of capturing photographs of a scene from the same location at different points in time (Hastings & Turner, 1965; Rogers et al., 1984). Repeat photography was first documented in central Europe, initially as a technique for tracking glacial change in the Alps, but it has since become an established method for documenting different types of ecological and

landscape change around the world (Webb et al., 2010). In recent decades, repeat photography studies have developed a variety of approaches to elicit information from oblique images and evaluate changes that have occurred between the time periods captured in each photograph. From early qualitative observations describing geomorphological and vegetative changes on the landscape (e.g., Byers, 2007; Gruell et al., 1982; Hastings & Turner, 1965), methods have evolved to include innovative quantitative approaches that generate measurable change metrics (e.g., Bayr & Puschmann, 2019; Rhemtulla et al., 2002; Roush et al., 2007).

Researchers undertaking quantitative analysis in repeat photography studies must perform two critical tasks: (1) identify and/or classify landcover information in the sequence of images; and (2) calculate the amount of detectable change. Oblique landscape photographs present several challenges to this process including perspective distortion, high interclass variation, image quality issues, and varying scales relative to pixel size (i.e., a pixel in the foreground of an image will capture less geographic area than a pixel in the background; Bayr & Puschmann, 2019; Clark & Hardegree, 2005; Kull, 2005; Sanseverino et al., 2016). Additionally, the oblique perspective of ground-based photographs does not allow for analysis using classification and change-detection techniques developed for nadir imagery (Bayr & Puschmann, 2019). Instead, studies have largely relied on manual photointerpretation techniques for measuring change.

Several different quantitative approaches have been used to analyze oblique images. For example, Rhemtulla et al. (2002) followed common aerial photographic interpretation techniques (i.e., hand-drawn polygons on acetate sheets overlaid on printed photographs) to delineate and categorize areas of homogenous landcover for image pairs. These data were then imported into a geographic information system (GIS), which allowed the authors to estimate relative vegetative change (as a percentage of *photograph area*) by summing pixels in image pairs by cover type (Rhemtulla et al., 2002). Fortin et al. (2019) modernized this approach by creating digital copies of image pairs and then manually classifying features of interest using a digitizing tablet and the Image Analysis Toolkit (IAT; custom software specifically developed for analyzing repeat photographs; Sanseverino et al., 2016). Hall (2001) and Roush et al. (2007) followed a different approach that overlaid a grid on top of image pairs and determined changes to vegetation cover per grid cell. More recently, Trant et al. (2020) used a digitizing tablet to delineate the treeline in 81 image pairs to assess high elevation ecosystem change. Other approaches have used a combination of image pairs and field observations to produce quantitative data (Hoffman & Todd, 2010; Masubelele et al., 2015; McClaran et al., 2010).

The different approaches for classifying landcover and calculating change between historical and repeat photographs emphasize two important shortcomings. The first is a reliance on manual photointerpretation to identify and categorize landcover information. Although this technique is an accurate approach (Wulder, 1998), it can be difficult to replicate and produce consistent results due to the subjectivity of different interpreters (Wulder et al., 2008). Manual photointerpretation is also a laborious, time-consuming, and expensive undertaking (Green, 2000). Recent studies have investigated the potential to use machine learning methods to classify information in oblique image pairs. Jean et al. (2015) developed an algorithm for classifying oblique photographs based on texture analysis using a machine learning segmentation algorithm that delineated "meta-categories" of forest and non-forest. Bayr and Puschmann (2019) used a deep learning algorithm to classify and evaluate woody vegetation change in pairs of repeat color photographs. However, both studies generated image classifications with coarse resolution limited to just two landcover categories and encountered challenges related to classifying historical grayscale photographs.

The second shortcoming concerns the difficulty of georeferencing oblique images, and therefore allowing absolute rather than relative quantitative comparison. To address this, Bozzini et al. (2012) developed the WSL Monoplotting Tool for georeferencing oblique photographs using photogrammetry methods, whereby each photographic pixel is plotted to its real-world location. Stockdale et al. (2015) used this tool to georeference landcover data derived from repeat photographs (manually interpreted using grid overlays) in a GIS at 100 m resolution. Recently, Bayr (2021) tested the accuracy of the monoplotting tool using a fine-resolution digital elevation model (DEM), reporting a mean displacement of 1.52 m for georeferenced points relative to their location in aerial photographs. However, the tool requires users to identify control points from features recognizable in both oblique photographs and nadir imagery, which can be difficult and time-consuming. This is especially true if the oblique photographs precede the nadir imagery by decades, which is often the case for historical images. Further, no repeat photography study has yet to develop a workflow that harnesses the potential of automated classification approaches in combination with georeferencing procedures to produce repeatable, accurate, and fine scale landcover change data.

To address this need, we have created an end-to-end workflow that deploys two recently developed custom software tools: a trainable segmentation network and

automated landcover classification algorithm, and a web-based georeferencing tool. These tools were developed by researchers associated with the Mountain Legacy Project (MLP; http://mountainlegacy.ca/), a research team that works with the world's largest collection of systematic high-resolution historic mountain photographs (Sanseverino et al., 2016). In this paper, we provide an overview of the two original tools and describe how they are implemented in a workflow for oblique photography analysis. To demonstrate the application of this workflow we produce a composite landcover map for a study area in Jasper National Park using images in the MLP collection. Our main purpose in this paper is to assess the performance of the tools and evaluate the accuracy of the map in relation to landcover data produced using more conventional techniques (i.e., supervised classification of 30 cm aerial imagery captured over the study area in 2020). The intent of this paper is to validate the new workflow for the purpose of producing landcover data from historical oblique photographs. This would benefit ecology and conservation by increasing the temporal depth of spatially explicit studies focused on understanding change dynamics in ecosystems and landscapes.

STUDY AREA

To assess the capability of the workflow to produce accurate georeferenced landcover data, we required a study area that had comprehensive oblique and orthographic photographic coverage. Jasper National Park extends over 11 000 km^2 of the eastern Canadian Rockies in west-central Alberta (Fig. 1). Established in 1907, it is the largest of a network of national, provincial, and wilderness parks that stretch along the continental divide on either side of the provincial border between Alberta and British Columbia. In 1915, the central portion of Jasper National Park was systematically photographed by Morrison Parsons Bridgland for the Dominion Land Survey (MacLaren et al., 2005). Bridgland established a network of 92 camera stations, typically on mountain peaks or prominent outcrops, from which he captured a total of 735 photographs (Rhemtulla et al., 2002). The photographs, along with horizontal and vertical measurements recorded with a theodolite, were then used to produce the first topographic maps for the area (Higgs, 2003; MacLaren et al., 2005). To the northeast of the Jasper townsite, several camera stations provide unobstructed and overlapping views of the Athabasca River valley, resulting in almost 100% coverage of the landscape (Fig. 1). This area was the focus of a repeat photography study by Rhemtulla et al. (2002) that evaluated 80 years of landcover change in the valley. In this paper we reanalyze the 2002 study

area using new repeat photographs captured in 2020 from Bridgland's original camera stations.

METHODS

Our workflow for producing landcover data features two new tools for oblique image classification and georeferencing. The Python Landscape Classifier (PyLC; https://github.com/scrose/pylc) is a trainable segmentation network that automates the classification of landcover types in grayscale and color oblique photographs (Rose, 2020). PyLC is based on an implementation of Deeplabv3+, a top performing deep convolution neural network (DCNN) optimized for semantic segmentation (i.e., each pixel in an image is assigned a class or label; Chen et al., 2017). The network was trained on 95 pairs of historical and repeat photographs from the MLP collection and their corresponding landcover classifications created by MLP researchers using manual classification (Fortin et al., 2019; Jean et al., 2015). PyLC classifies images into 8 landcover classes originally defined by Jean et al. (2015) and based on the broad habitat categories found in the Canadian Rockies (Table 1). Data augmentation (i.e., geometric manipulations of training samples) was used to increase underrepresented classes in the training dataset to mitigate class imbalance (Table 1). This technique produced modest improvements to overall accuracy (+3% historic/+1% repeat), but much larger gains for underrepresented classes (Rose, 2020). Rose (2020) reported that the top performing models produced overall weighted F1 scores (a measure of the overlap between a segmentation mask and a manually classified mask) of 0.841 for historical photographs, and 0.909 for contemporary repeat photographs.

The georeferencing tool uses a new approach to relate landcover classifications derived from an oblique photograph to its correct geographic location (Higgs et al., 2020). The tool utilizes a web-based ray tracing algorithm to establish a correspondence between each image pixel and DEM cell. The tool requires information from the original photograph (camera location, azimuth of the camera orientation, the lens field of view (FOV), and the image dimensions) and a fine-resolution elevation data. The landcover classification from the photograph is georeferenced in three steps (Fig. 3). The algorithm generates a "virtual" version of an oblique photograph by tracing rays from the camera FOV to visible pixels (viewed as virtual columns) in a DEM (Fig. 3). The original photograph is then aligned to the virtual photograph using control points and a perspective transformation. Finally, the algorithm exploits the relationship between the classified image (which shares the same dimensions as the
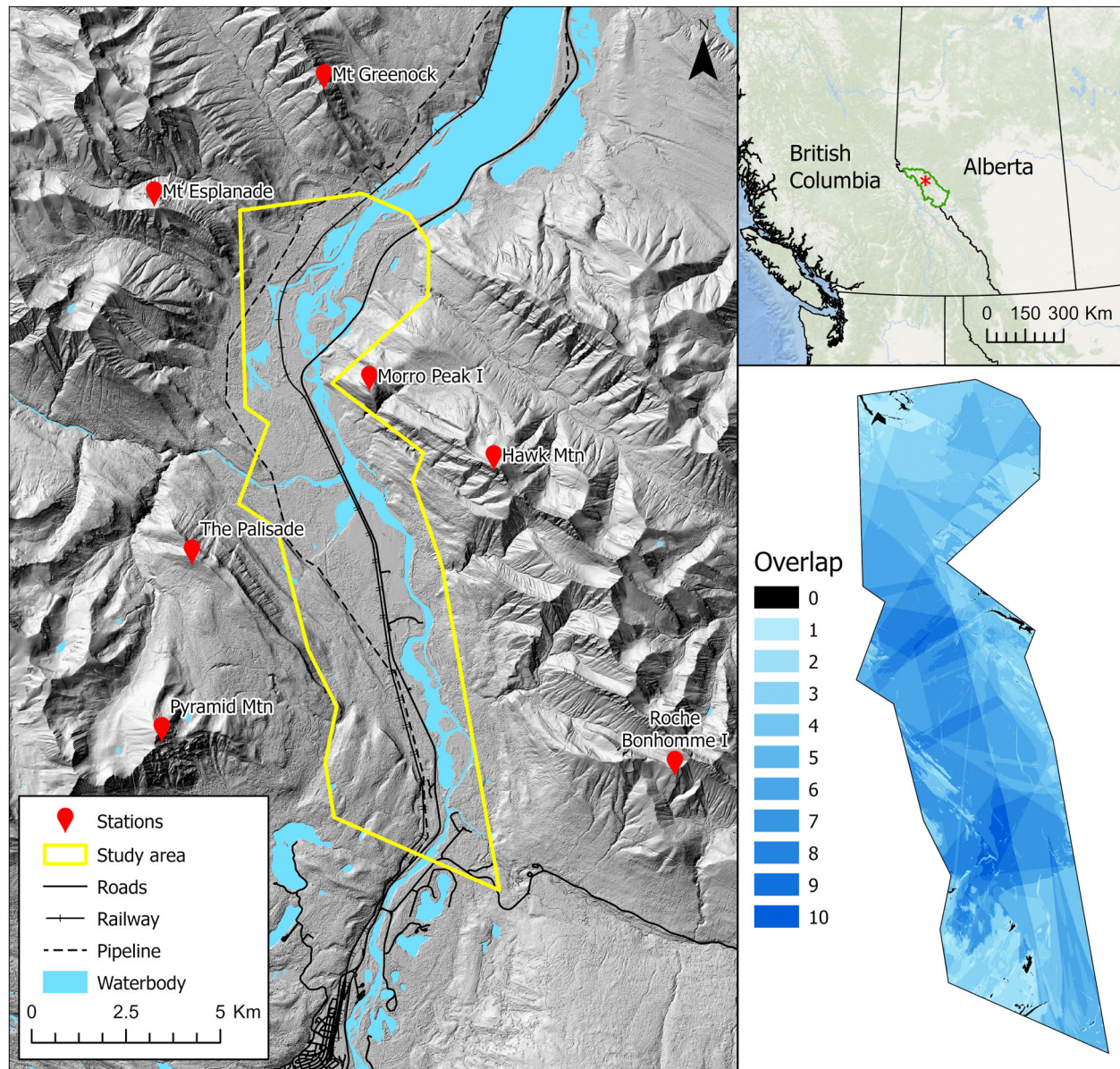
Figure 1. Map of the Athabasca River valley study area and camera station locations in Jasper National Park. Top right inset: location of study area (red star) and Jasper National Park (green) in Western Canada. Bottom right inset: Amount of field of view overlap for the 19 images used in the analysis. Map credits: ESRI, 2021; Natural Resources Canada, 2021.

original photograph) and the DEM to plot the landcover values in real-world space.

To assess the capability of PyLC and the IAT georeferencing tool to produce accurate landcover data, we undertook fieldwork in August/September 2020 to capture third sequential repeat photographs (original 1915; first repeats 1998/99) overlooking the study area. We required new repeat photographs because the first repeats were captured on black and white film and do not have the required spectral information for analysis using the

current version of PyLC. Photographs were taken with a 51.4-megapixel FujiFilm GFX50s medium format digital camera with a 32–64 mm F4 zoom lens, and a Novoflex panoramic head and tripod. Field notes and location photographs (i.e., for camera tripod placement) recorded by Rhemtulla et al. (2002) were instrumental in planning and navigating to original station locations. Gridded printouts of the historic photographs were used to fine-tune the tripod position and align each repeat photograph through the camera viewfinder. Detailed field notes

TABLE 1. Description of land cover categories for PyLC/SVM classification scheme. Percent change indicates adjustments to pixel class distribution after data augmentation. SVM samples indicate the number of training samples per class used by the SVM classifier to generate the orthogonal land cover map. Adapted from Rose, 2020.

Category	Description	Pixel distribution	Augmented pixel dist.	Percent change	SVM samples
Coniferous forest	Greater than 75% coniferous trees	0.219	0.2431	11	20
Barren ground	Soil, sand, gravel, or rock	0.1155	0.1149	−0.5	44
Water	Lakes and rivers	0.0008	0.0042	401	94
Regenerating area	Visibly recently burned forest	0.021	0.0748	255.5	N/A
Herbaceous/shrub	Shrubs, grasses, and herbaceous vegetation	0.0613	0.0638	4.1	49
Wetland	Vegetation with a wet or aquatic moisture regime	0.0082	0.0388	370.8	22
Broadleaf/ mixedwood	>70% broadleaf trees/patches with 30%–70% broadleaf cover and the rest coniferous trees and/or shrub	0.0095	0.0493	419.4	44
Snow/ice	Snow and ice	0.008	0.0203	155.9	N/A
Non categorized	Non categorized	0.5568	0.3909	−29.8	N/A

including coordinates of camera location using a Garmin GPS and azimuth for each photograph using a Brunton transit were recorded to assist with later georeferencing tasks. Seven survey stations, each comprising multiple photographs (5 to 12 photos per station), were revisited yielding a total of 69 repeat photographs (Fig. 1).

High-resolution elevation data derived from airborne LiDAR were obtained from Natural Resources Canada (2021) and Jasper National Park. These data were formatted, mosaicked, and resampled to 2 m resolution to produce a 30 × 40 km digital surface model (DSM) and digital terrain model (DTM) for the study area (all GIS tasks were performed in ArcGIS Pro 2.8.3; ESRI, 2021). Note that the DSM produces more realistic virtual photographs by including surface features such as trees, which can be used for alignment with the same trees in the oblique photograph. The DTM is then used for georeferencing the classified images (avoiding the speckle effect that would be present if using the DSM). To determine which station photographs to include in this analysis, viewsheds were generated for each of the 69 photographs using the Viewshed tool (ESRI, 2021). Only image viewsheds that had a considerable spatial footprint within the study area were selected, which reduced the total number of images to 19 (providing 99.3% coverage of the study area; Fig. 1; Appendix A). We then classified landcover in each of the 19 images with PyLC using the landcover classes listed in Figure 2 (Appendix B).

The 19 classified images produced by PyLC were then georeferenced with the IAT georeferencing tool using the elevation data and camera metadata (see steps described in Fig. 3; Appendix C). To account for overlap between the georeferenced images, all 19 viewsheds were combined in ArcGIS Pro 2.8.3 using the cell statistics tool (ESRI, 2021) with the majority overlay statistic selected

(i.e., the value that occurs most often for cells with multiple values). Where cells had multiple majority values, the tool produced a no data value, leading to only 91.7% coverage of the study area. To address this, classified images were dropped iteratively based on a visual assessment of PyLC output quality with the majority cell value recalculated each time until two viewsheds remained. The resulting 19 grids were then mosaicked together in the order they were produced using the Mosaic to New Raster tool (ESRI, 2021). This process brought the coverage of the study area back up to 99.3%. The remaining unclassified cells were filled using their nearest neighbor values with the Nibble tool (ESRI, 2021). Several areas of water were misclassified as snow/ice in the study area – these areas were reclassified back to water using the Reclassify tool (based on the assumption that there is no ice in the valley bottom during the summer months; ESRI, 2021). Similarly, areas of regeneration were reclassified to conifer as there have been no recorded wildfires within the study area for decades. The final step for producing the oblique landcover map involved clipping the grid to the study area extent (Appendix D).
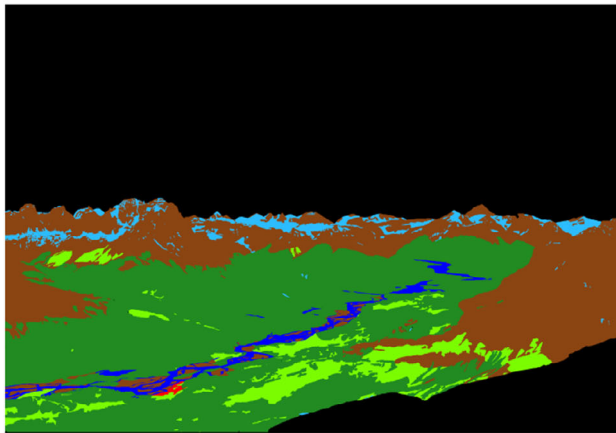
The accuracy of the IAT georeferencing tool was assessed using one georeferenced image from each of the seven camera stations. Eight test points were manually digitized on each georeferenced image using identifiable features within the study area. Control points for the same features were then digitized on 30 cm RGBI high-resolution aerial imagery obtained from Jasper National Park captured over the study area in 2020. We determined georeferencing error by calculating the root-mean-square error (RMSE) for each set of test and control points. To compare accuracy with the WSL tool, we also calculated the point displacement by measuring the Euclidian distance between the test and control points
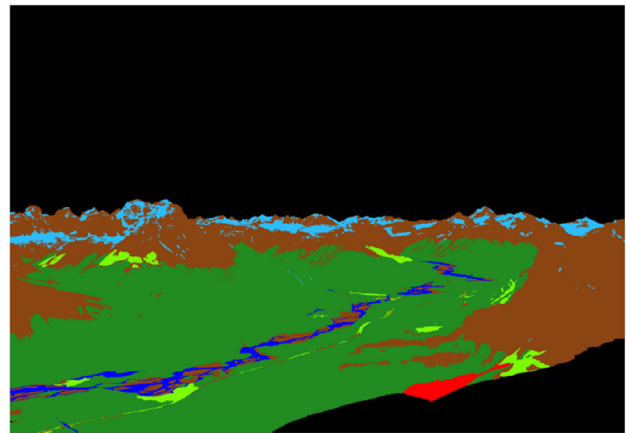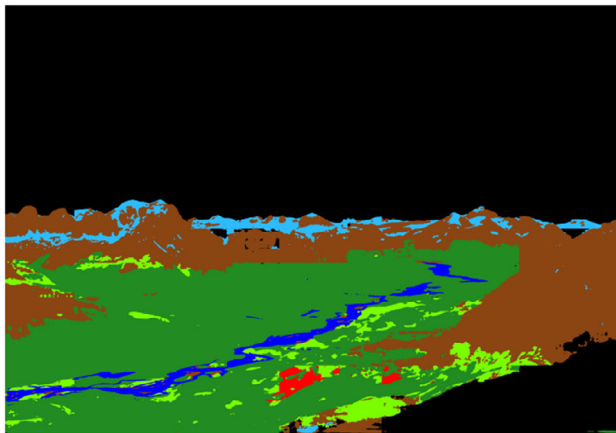
Historical image
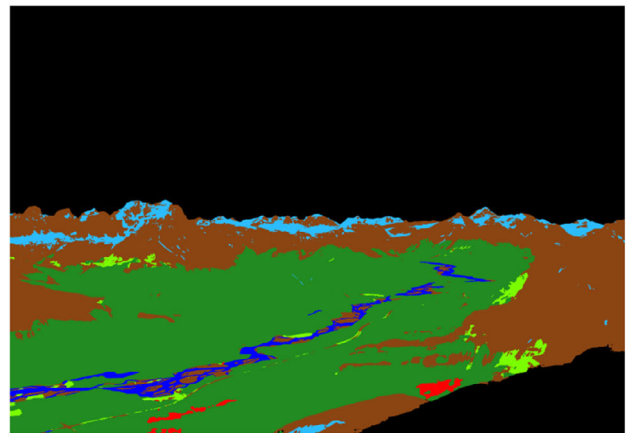
Repeat image

Manual classification

Manual classification

PyLC classification

PyLC classification

Coniferous forest — Regenerating areas — Broadleaf/mixedwood
Barren ground — Herbaceous/shrub — Snow/ice
Water — Wetland

Figure 2. Examples of image classifications produced by manual methods and PyLC for historical and repeat photograph pairs. Classification accuracy was typically better for repeat photographs due to the higher image quality and richer spectral information. Figure adapted from Rose (2020).

(Bayr, 2021). Finally, we measured the distance and angle of incidence between all camera locations and their associated test points to evaluate their influence on point displacement (Stockdale et al., 2015). A Generalized Linear Model was constructed in ArcGIS Pro 2.8.3, using the following equation:

$$\begin{aligned} \text{point displacement(m)} = &\ \text{intercept} \\ &+ \beta_1(\text{distance to camera}) \\ &+ \beta_2(\text{angle of incidence}) \end{aligned}$$

To satisfy model assumptions, the mean displacement values for each image were fit to a normal distribution using a square root transformation.

We compared the oblique landcover map with landcover data produced from the 30 cm RGBI high-resolution aerial imagery using a Support Vector Machine (SVM) classifier in ArcGIS Pro 2.8.3 (ESRI, 2021). SVMs are supervised machine learning algorithms optimized for locating exemplars (i.e., support vectors) that form decision boundaries for separating landcover classes (Pal & Mather, 2006). The SVM classifier was trained with samples of land cover from the aerial imagery using the same classification scheme used for producing the oblique land cover map (excluding snow/ice and regenerating areas). A total of 273 samples were identified and their distribution across the 6 land cover classes are reported in Table 1. The results were resampled to 2 m using bilinear interpolation (Appendix D).

We compared accuracy of the landcover maps generated from the oblique and orthogonal imagery based on reference data derived from the 30 cm aerial imagery. We generated 198 equalized stratified random points (i.e., randomly distributed points within each class, in which each class has the same number of points to mitigate class size imbalances) in ArcGIS Pro 2.8.3 and extracted the landcover values from the two maps at each point (ESRI, 2021). We interpreted reference landcover values for each random point by visually assessing the aerial imagery. We then used these data to compute a confusion matrix for each landcover map, which showed the overall accuracy based on the percentage of correctly classified samples. User's accuracy (i.e., the probability that features on the map are present on the ground) and producer's accuracy (i.e., the probability that features on the ground are correctly shown on the map) were reported for each class.

RESULTS

The RMSE for the subset of 7 individual images used to assess georeferencing accuracy ranged from 2.8 to 7.7 m, with an overall mean of 4.6 m (Table 2). The mean displacement between test and control points ranged from 1.8 to 6.9 m, with a mean of 3.7 m (SD = 2.2 m; Table 2). The distance from camera to test points ranged from 1647.7 m to 10 512.9 m, with a mean of 5832.6 m; and the angle of incidence ranged from 5.9° to 23.2°, with a mean of 13.6°. Based on the results of the GLM, there was no significant effect of distance to camera ($P = 0.84$, $\alpha = 0.05$) and angle of incidence ($P = 0.29$, $\alpha = 0.05$) on the mean point displacement.
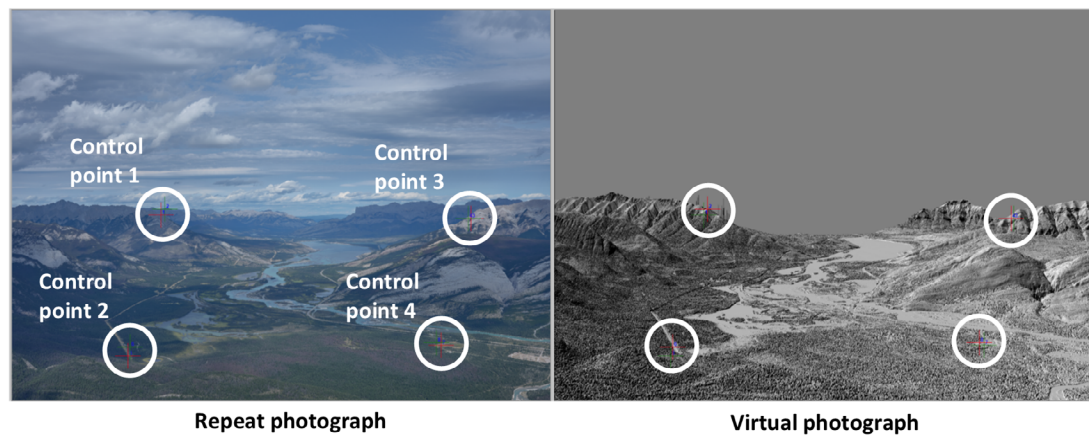
The two landcover maps are largely consistent in depicting the dominant features of the landscape. Both maps were proficient in classifying the Athabasca River and other water bodies, the open swaths of herbaceous/shrub in the center of the study area, and patches of broadleaf/mixedwood in the northern extent (Fig. 4). However, the grain of the two maps is noticeably different owing to the different approaches used. The oblique land cover map is smoother in appearance and presents a more generalized view of the study area. Comparatively, the orthogonal land cover map has the classic speckled appearance of a pixel-based classification and captures more detail on the landscape. This is evidenced by the completeness of the water bodies and linear features, and an overall trend of intermixed classes, specifically where herbaceous/shrub intermixes with barren ground and conifer. However, the latter approach incorrectly classified considerably more broadleaf/mixedwood in the study area because of class confusion with coniferous forest. Wetland was also overclassified consistently throughout the study due to confusion with coniferous forest, herbaceous/shrub, and barren ground.

In terms of landcover class distribution, barren ground and water shared similar proportions for the two landcover maps while there were considerable differences in the proportions of the other four landcover classes (Fig. 5). The biggest difference was for coniferous forest: the oblique landcover map classified 72.3% of the study area as coniferous forest versus 45.2% for the orthogonal map. However, the orthogonal landcover map classified substantially more broadleaf/mixed wood (16.3%) than the oblique map (1.5%). The orthogonal landcover map

Step 1—Building the virtual photograph

Digital surface model

Hillshade model

Virtual photograph
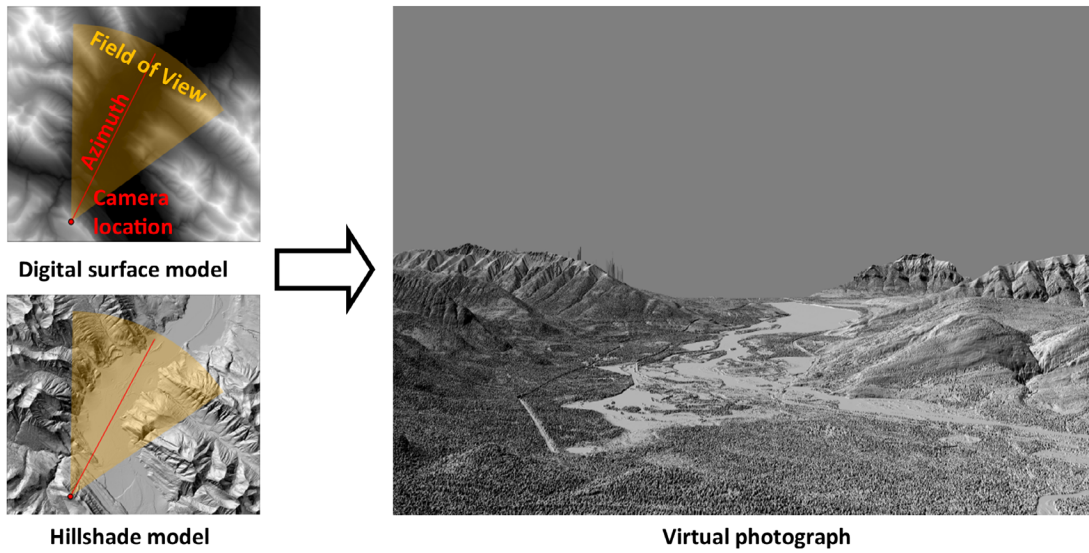
Step 2—Aligning the repeat and virtual photographs

Repeat photograph

Virtual photograph

Step 3—Producing the georeferenced viewshed

Digital terrain model

Aligned image classification

Georeferenced viewshed

- Coniferous forest
- Barren ground
- Water
- Regenerating area
- Upland herbaceous
- Wetland
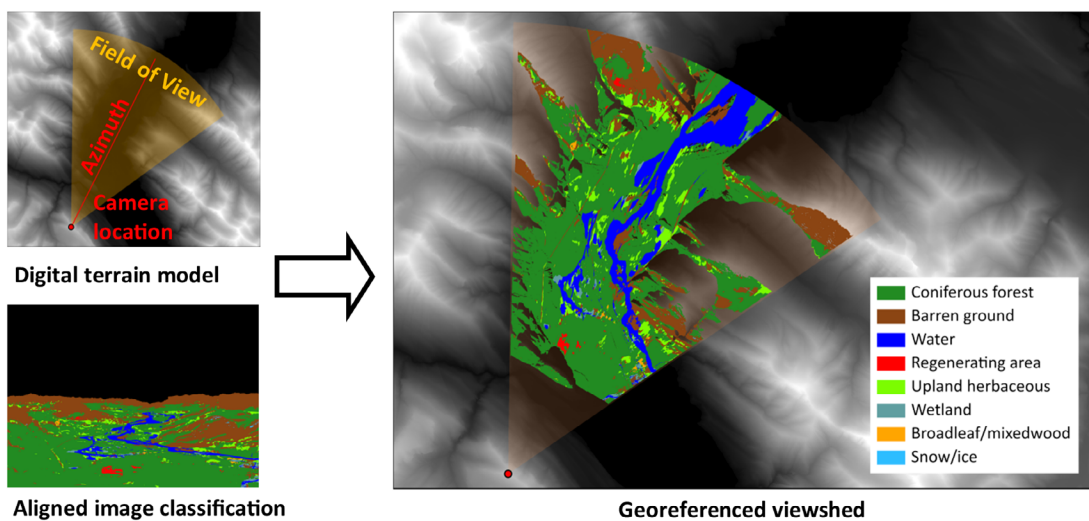- Broadleaf/mixedwood
- Snow/ice

Figure 3. Steps for georeferencing classified photographs in IAT. Step 1: a virtual photograph, replicating the original photograph FOV, is produced using camera metadata and a DEM. Step 2: the original photograph is aligned to the virtual photograph using control points and a perspective transformation, which are then used to align the image classification to the virtual photograph. Step 3: the cell values from the aligned image classification are then georeferenced by exploiting the relationship between the virtual photograph and elevation data.

TABLE 2. Mean georeferencing error (i.e., point displacement) based on 8 test points per image, and mean distance of points from camera and angle of incidence.

Station/Image#	Root mean square error (m)	Mean point displacement (m) (±SD)	Mean distance (m) (range)	AOI (°) (range)
Hawk DSCF0614	3.8	1.8 (±0.6)	4785.5 (3936.3–5955.7)	19.2 (14.9–23.2)
Pyramid DSCF0782	2.8	2.4 (±1.4)	7426.9 (6766.5–8206.9)	13.7 (12.3–15)
Esplanade DSCF0663	4.0	3.5 (±2.1)	5934.4 (4241–8244.4)	13.2 (8.9–17.6)
Palisade DSCF0838	4.6	3.8 (±2.8)	5616.2 (4490–7087)	12.1 (9.4–14.8)
Morro I DSCF0575	4.7	4.1 (±2.2)	2714.5 (1647.7–3267.4)	15.1 (11.9–24)
Greenock DSCF0547	3.6	3.2 (±2)	6983.2 (4263–10512.9)	9.8 (5.9–14.9)
Bonhomme I DSCF725	7.7	6.9 (±4.1)	7367.5 (5388.9–9561.4)	11.7 (7.1–16)
Mean	4.6	3.7 (±2.2)	5832.6	13.6

also classified more wetland (7.9%) and herbaceous/shrub (5.7%) than the oblique landcover map.

The overall accuracy of the oblique landcover map was 68% (Table 3). User's accuracy produced scores above 75% for four of the map classes. However, barren ground (51%) and wetland (33%) had low user accuracy, with the latter class typically misclassified as either herbaceous/shrub or barren ground. Scores for producer's accuracy were more erratic: broadleaf/mixed wood (90%) and water (90%) scored highest; the lowest classes were herbaceous/shrub (55%) and barren ground (49%). The broadleaf/mixed wood and water classes achieved high scores for both producer's and user's accuracy. User's accuracy for the conifer class was 79%, but producer's accuracy was lower due to class confusion with barren ground. There was a larger contrast in scores for herbaceous/shrub, with a high user's accuracy (79%) whereas producer's accuracy (55%) was affected by class confusion with wetland and barren ground.

The orthogonal landcover map had an overall accuracy of 60% (Table 4) based on the same accuracy assessment points generated for the map derived from oblique photographs. Water (85%) had the highest user's accuracy score, and wetland (38%) had the lowest. Notably, conifer (48%) was frequently misclassified as broadleaf/mixed wood. Similarly, for producer's accuracy, water (93%) scored highest, and wetland (29%) was lowest.

DISCUSSION

The results of the accuracy assessment indicate the strong potential of a new workflow for oblique photography

analysis. When compared to studies georeferencing MLP images with the WSL monoplotting tool, the mean displacement error (3.7 m) for this analysis was considerably lower than Stockdale et al. (2015) and McCaffrey and Hopkinson (2017) who found error values of 14.7 and 21.7 m, respectively. A more recent WSL monoplotting assessment by Bayr (2021) did produce a lower mean displacement error value (1.52 m), but the authors used images taken from lower elevations that were closer to features of interest on the landscape compared to the images in the current study. The steps for georeferencing an image using the IAT georeferencing tool are arguably more intuitive than the WSL monoplotting tool, as (1) fewer control points are required, (2) the reference data (i.e., the virtual photo) shares the same oblique view as the image to be georeferenced, which makes selection of reciprocal control points more intuitive, and (3) the sweep function allows for immediate visual assessment of alignment accuracy. However, there are drawbacks related to the requirement of precise camera station metadata to accurately plot the image classifications. Imprecise camera azimuth and/or coordinates require time-consuming adjustments to produce the optimal virtual photograph for georeferencing. There are opportunities to further develop the IAT georeferencing tool to streamline the adjustment process for existing repeat photograph pairs. New repeat photography fieldwork can also address this issue by using precision instruments to accurately record camera metadata such as survey-grade transits (incorporated into the camera head) and sub-meter GPS units that utilize correction services (Walter, 2020).
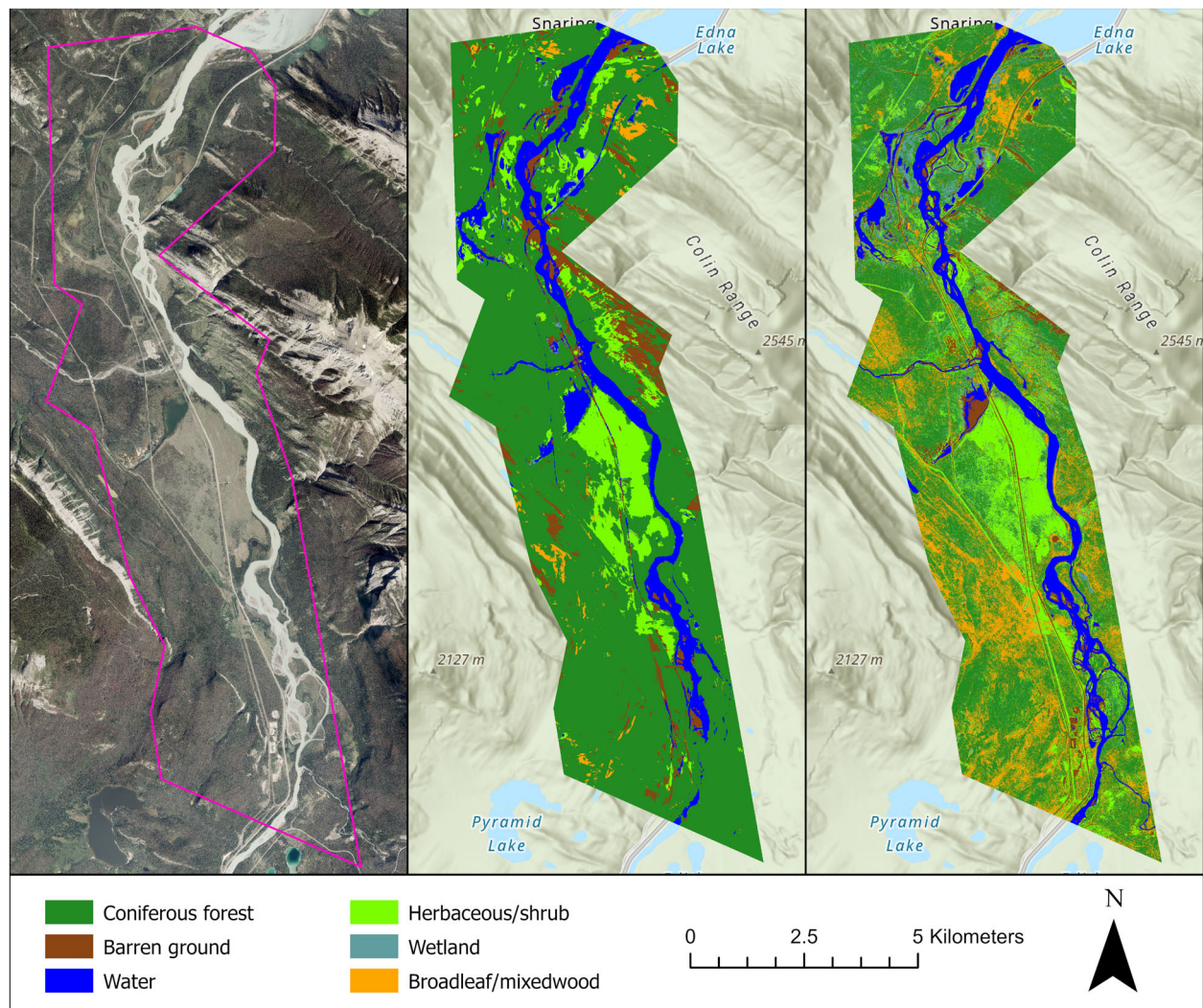
Figure 4. Landcover maps produced for the Athabasca River valley study area. Left panel: 30 cm high-resolution aerial image. Middle panel: landcover map produced using oblique photographs (2 m resolution). Right panel: landcover map produced using orthogonal imagery (30 cm resolution). Map credit: ESRI, 2021.

The oblique landcover map produced from the oblique images successfully depicted the dominant features of the study area despite a moderate overall score in the accuracy assessment. While several classes produced high scores for both producer's and user's accuracy, the overall accuracy score was impacted by low scores for two classes: wetland and barren ground. Wetland is a challenging class to categorize, for both oblique and orthogonal imagery, given its similarities to other non-wetland classes (Mahdavi et al., 2018). This issue is reflected in class confusion with herbaceous/shrub in the results. Classification accuracy for barren ground was hampered by confusion with numerous classes, especially conifer and wetland. Confusion with the conifer class may be explained by "shadow effect" where patches of barren ground between trees are obscured due to the oblique angle of the photographs. There was also a significant outbreak of mountain pine beetle in the park over the last decade, and the reddish-brown color of beetle-killed pine trees may also have been misclassified as barren ground. A final issue arises from including roads and campgrounds in the barren ground class—these features were often misclassified as wetland as described above.

Comparatively, the overall accuracy for the orthogonal landcover map was lower than the oblique landcover map. The orthogonal landcover map did produce the highest score for an individual class (water), and the SVM algorithm produced better results when classifying
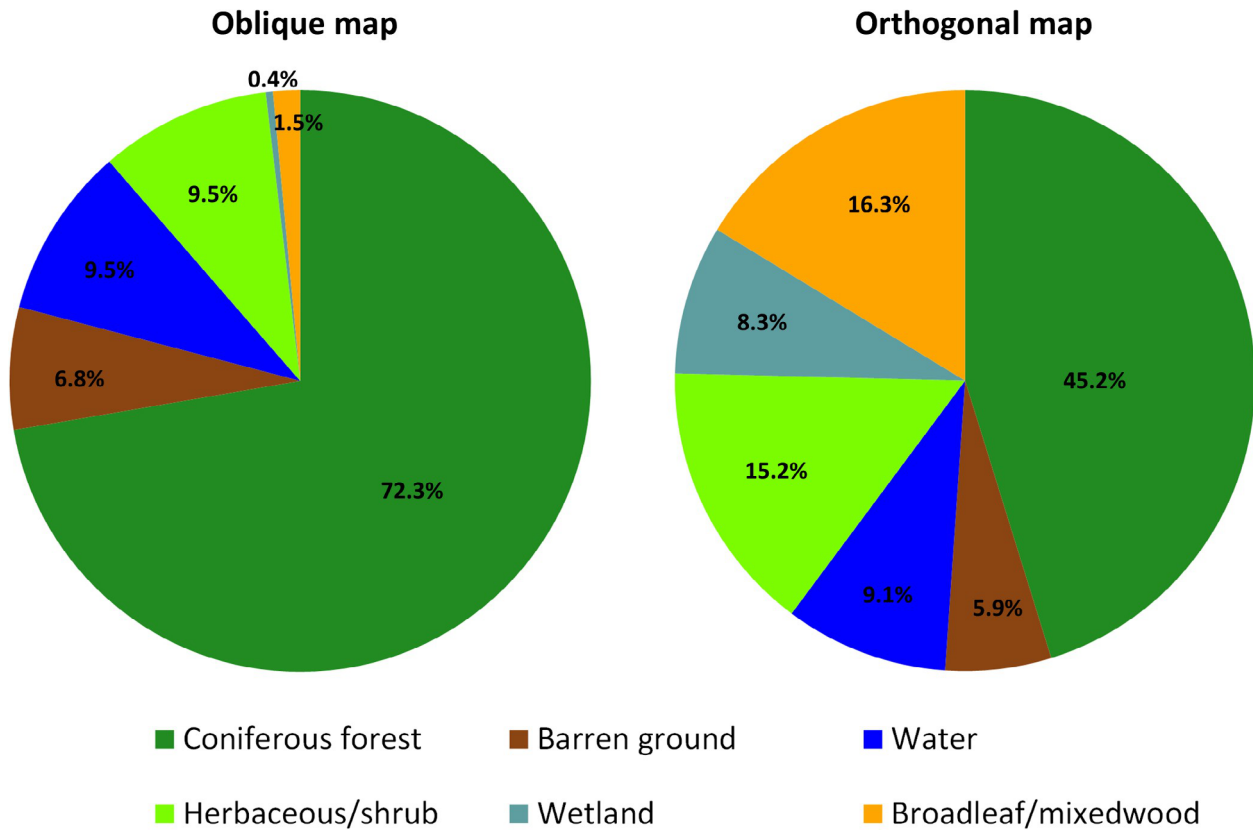
© 2023 The Authors. *Remote Sensing in Ecology and Conservation* published by John Wiley & Sons Ltd on behalf of Zoological Society of London.

Figure 5. Proportion of landcover classes (%) for the oblique and orthogonal maps.

TABLE 3. Confusion matrix for the oblique landcover map compared to reference aerial imagery indicating overall accuracy of 68%.

Class	Conifer forest	Barren ground	Water	Herbaceous/ shrub	Wetland	Broadleaf/ mixedwood	Total	U accuracy
Coniferous forest	26	2	0	3	1	1	33	0.79
Barren ground	6	17	0	5	3	2	33	0.51
Water	0	5	27	1	0	0	33	0.82
Herbaceous/ shrub	0	3	0	26	4	0	33	0.79
Wetland	1	8	3	10	11	0	33	0.33
Broadleaf/mixed	3	0	0	2	0	28	33	0.85
Total	36	35	30	47	19	31	198	
P Accuracy	0.72	0.49	0.90	0.55	0.58	0.90		0.68

TABLE 4. Confusion matrix for the orthogonal landcover map compared to reference aerial imagery indicating overall accuracy of 60%.

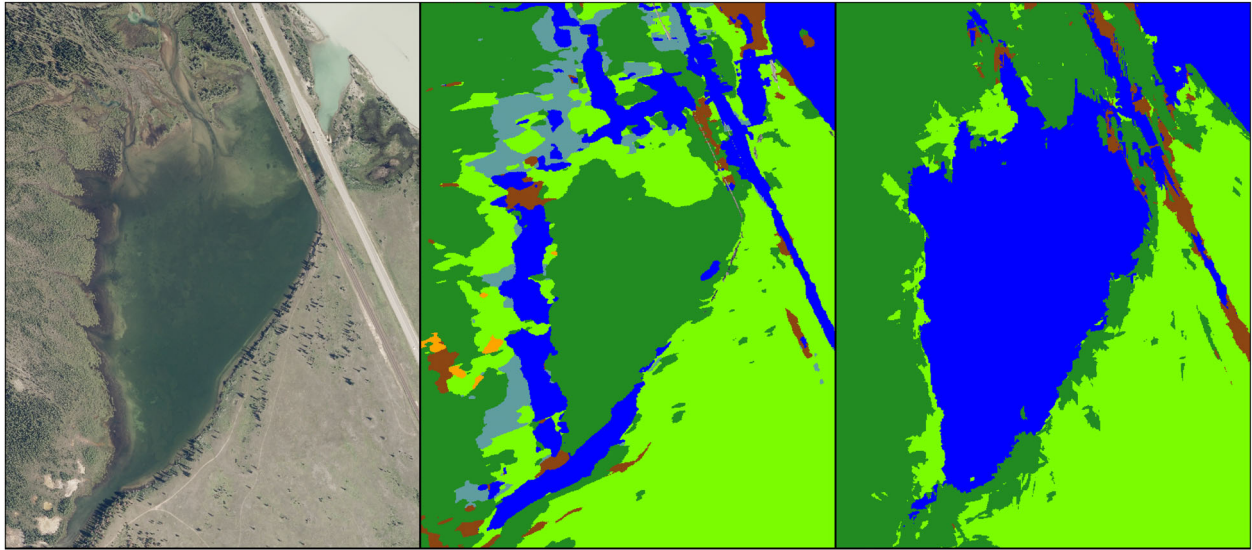| Class	Conifer forest	Barren ground	Water	Herbaceous/shrub	Wetland	Broadleaf/mixedwood	Total	U accuracy
Coniferous forest	25	2	0	5	3	17	52	0.48
Barren ground	1	18	2	2	4	0	27	0.67
Water	0	0	28	0	5	0	33	0.85
Herbaceous/shrub	5	15	0	27	0	1	48	0.56
Wetland	2	1	0	4	5	1	13	0.38
Broadleaf/mixed	3	0	0	6	0	16	25	0.64
Total	36	36	30	44	17	35	198	
P Accuracy	0.69	0.5	0.93	0.61	0.29	0.46		0.60

Figure 6. Example of a classification error in an individual georeferenced image classification that was corrected when mosaicking all georeferenced image classifications together using the mode value technique. Left panel: orthophoto showing the extent of the lake. Middle panel: the lake is misclassified as conifer in single georeferenced image classification (derived from a photograph captured from the Hawk Mountain station). Right panel: the lake is correctly classified as water in the oblique landcover map comprising 19 georeferenced image classifications.

barren ground. However, the algorithm was inconsistent when classifying conifer due to a high amount of class confusion with broadleaf/mixed wood forest. This may relate to coniferous trees at different stages of growth (i.e., more open or patchy) confusing the algorithm (whereas this would be less of an issue when viewing coniferous stands at an oblique angle). Similarly, there was considerable class confusion between herbaceous/shrub and barren ground, which may relate to the many areas within the study area where these two classes are intermixed.

A key advantage of the workflow described in this paper is the speed, efficiency, and consistency of classifying images using PyLC. However, noticeable errors are present in the image classifications and the results indicate that PyLC often confused wetland and barren ground with other classes. These errors and misclassifications could be explained by the data used to train PyLC (although georeferencing error may contribute to classification error too). At present the manually classified training datasets constitute less than 0.1% of the complete MLP image collection, and they do not represent the full variety landcover found throughout the region. For example, > 50% of the training data is from the Willmore Wilderness Park in western Alberta, where there is a dearth of anthropogenic features. This bottleneck of representative training data limits model sensitivity or classifying additional landcover classes—a more robust model

requires a wider range of photographs/classifications to be included in the training data.

Improving PyLC accuracy could be addressed in several ways. Manually corrected PyLC classifications are considerably quicker to produce than full manual classifications and could be an effective approach to expanding training datasets (especially for underrepresented ecoregions in the Canadian cordillera). Corrections typically require 1–3 h of work per image and can be performed using photo-editing software applications. Additionally, further work to refine data augmentation methods can potentially address a severe class imbalance in the training data sets, as can models optimized for classifying specific environments. The addition of new landcover classes (i.e., developed areas/infrastructure, mountain pine beetle impacted forest, etc.) may improve the classification accuracy for other classes. Finally, PyLC improvements that incorporate semi-supervised approaches to segmentation have the potential to reduce reliance on labeled training data (Hong et al., 2015; Hung et al., 2018). Further, unsupervised segmentation approaches employing iterative self-training procedures have potential to eliminate the need for training data altogether (Zou et al., 2018).

The mosaicking method for combining the 19 georeferenced image classifications makes it challenging to track the source of error in the oblique landcover map. However, this approach can correct misclassification errors from individual images when they are mosaicked together

using the mode value technique. An example demonstrating the advantage of this method is found at a lake located to the south of the Snaring River mouth (Fig. 6). One of the classified images from the Hawk Mountain station incorrectly classifies the lake as conifer, whereas this error is corrected in the combined oblique landcover map. Another advantage of this approach is the mitigation of the shadow effect of the oblique photographs, whereby landcover in the viewshed is obscured by trees or elevated terrain. Combining georeferenced images from different angles in the study area can fill in these gaps and address issues where the height of trees from the oblique angle does not result in an exaggerated footprint on the landscape.

Other important considerations for the workflow detailed in this paper relate to image quality, DEM resolution, and the terrain of prospective study areas. While PyLC is capable of classifying images of varying quality (i.e., images captured with sub-optimal lighting), some images do not lend themselves well to classification due to the elevation of camera station relative to the landscape below, foreground vegetation obscuring large parts of the field of view, or simply the distance from the camera to the landcover area of interest. The accuracy of the georeferenced image classifications is largely related to the resolution of the DEM employed by the IAT georeferencing tool. To date, there is limited coverage of fine-resolution LiDAR-derived DEM data in the Canadian Rockies and other mountainous regions in western Canada. The availability of high-resolution elevation data should be considered when undertaking such work for a specific area. Another consideration is the elevation of prospective study sites. The analysis presented in this paper is focused on subalpine valley ecosystems, but the real potential of these methods may lie in alpine environments where the oblique angle of the photographs can offer richer detail than orthogonal imagery (Fortin et al., 2019). This would be especially true for ecotone shift assessments (i.e., McCaffrey & Hopkinson, 2020; Peterson et al., 2022; Trant et al., 2020).

A logical next step is applying the workflow presented in this paper to historical survey photographs in the MLP collection captured between 1880 and 1950. This information would predate the first aerial imagery surveys by decades and would deepen existing monitoring reference data, providing insights into the configuration and composition of ecosystems under historically contingent disturbance regimes (Keane et al., 2009). Quantifying the historical range of variability for ecosystems (i.e., Landres et al., 1999) can provide a spatially explicit baseline for evaluating future responses to altered disturbance regimes, climate warming, and other anthropogenic stressors (Turner & Seidl, 2023). However, different machine learning models are required

to classify color (3-band) and grayscale (single band) images. While PyLC models configured for classifying historical photographs have been developed (Rose, 2020), the image classifications produced from historical grayscale photographs presently lack the accuracy and consistency of the classifications produced from their color counterparts. Work is underway to improve machine learning approaches to historical imagery.

In conclusion, the new workflow described in this paper advances the use of oblique photographs to yield quantitative landcover data. Our approach has several advantages over existing methods, specifically the ability to produce quick and consistent image classifications with little human input, and accurately georeference and combine these classifications to generate landcover data for large areas. We have demonstrated that this approach produces results of comparable accuracy to landcover maps generated using supervised classification and orthogonal imagery. Further developments for improving this workflow would be best focused on three areas: (1) expanding training data for PyLC that includes new landcover classes; (2) improving the performance of PyLC algorithm (i.e., incorporating updates to Deeplabv3+); and (3) increasing the accuracy of camera station metadata to expedite georeferencing tasks. Additionally, new research is required to investigate the potential of this new workflow to support management practices in protected areas. Historical and repeat landcover maps derived from oblique photographs can provide valuable data for vegetation monitoring, restoration activities, and management planning in an era of rapid change.

ACKNOWLEDGMENTS

REFERENCES

Bayr, U. (2021) Quantifying historical landscape change with repeat photography: an accuracy assessment of geospatial data obtained through monoplotting. *International Journal of Geographical Information Science*, **35**(10), 2026–2046. Available from: https://doi.org/10.1080/13658816.2021.1871910

Bayr, U. & Puschmann, O. (2019) Automatic detection of woody vegetation in repeat landscape photographs using a convolutional neural network. *Ecological Informatics*, **50**, 220–233. Available from: https://doi.org/10.1016/j.ecoinf.2019.01.012

Bozzini, C., Conedera, M. & Krebs, P. (2012) A new monoplotting tool to extract georeferenced vector data and orthorectified raster data from oblique non-metric photographs. *International Journal of Heritage in the Digital Era*, **1**(3), 499–518. Available from: https://doi.org/10.1260/2047-4970.1.3.499

Byers, A.C. (2007) An assessment of contemporary glacier fluctuations in Nepal's Khumbu Himal using repeat photography. *Himalayan Journal of Sciences*, **4**(6), 21–26. Available from: https://doi.org/10.3126/hjs.v4i6.979

Chen, L.-C., Papandreou, G., Kokkinos, I., Murphy, K. & Yuille, A.L. (2017) DeepLab: semantic image segmentation with deep convolutional nets, Atrous convolution, and fully connected CRFs. *IEEE Transactions on Pattern Analysis and Machine Intelligence*, **40**(4), 834–848.

Clark, P.E. & Hardegree, S.P. (2005) Quantifying vegetation change by point sampling landscape photography time series. *Rangeland Ecology & Management*, **58**(6), 588–597. Available from: https://doi.org/10.2111/04-111R2.1

ESRI. (2021) *ArcGIS pro: release 2.8.3*. Redlands, CA: Environmental Systems Research Institute.

Fortin, J.A., Fisher, J.T., Rhemtulla, J.M. & Higgs, E.S. (2019) Estimates of landscape composition from terrestrial oblique photographs suggest homogenization of Rocky Mountain landscapes over the last century. *Remote Sensing in Ecology and Conservation*, **5**(3), 224–236. Available from: https://doi.org/10.1002/rse2.100

Green, K. (2000) Selecting and interpreting high-resolution images. *Journal of Forestry*, **98**(6), 37–40. Available from: https://doi.org/10.1093/jof/98.6.37

Gruell, G.E. (1983) *Fire and vegetative trends in the northern Rockies: interpretations from 1871–1982 photographs*. General technical report INT-158. Ogden, UT: U.S. Department of Agriculture, Forest Service, Intermountain Forest and Range Experiment Station.

Gruell, G.E., Schmidt, W.C., Arno, S.F. & Reich, W.J. (1982) *Seventy years of vegetative change in a managed ponderosa pine Forest in Western Montana—implications for resource management*. Ogden, Utah: U.S. Department of Agriculture, Forest Service, Intermountain Forest and Range Experiment Station.

Hall, F.C. (2001) *Ground-based photographic monitoring*. General Technical Report PNW-GTR-503. Portland, OR: U.S. Department of Agriculture, Forest Service, Pacific Northwest Research Station, p. 340.

Hastings, J.R. & Turner, R.M. (1965) *The changing mile. An ecological study of vegetation change with time in the lower mile of an arid and semiarid region*. Tucson, Arizona:
University of Arizona Press. https://www.cabdirect.org/cabdirect/abstract/19670700517

Hayward, G.D., Veblen, T.T., Suring, L.H. & Davis, B. (2012) Challenges in the application of historical range of variation to conservation and land management. In: Wiens, J.A., Hayward, G.D., Safford, H.D. & Giffen, C.M. (Eds.) *Historical environmental variation in conservation and natural resource management*. Hoboken, NJ: Wiley-Blackwell, pp. 32–45.

Higgs, E. (2003) *Nature by design: people, natural process, and ecological restoration*. Cambridge, MA: MIT Press.

Higgs, E.S., Sanseverino, M.E., Whitney, M.J. & Fortin, J. (2020) *Advances in visual applications: Visualizing & Quantifying Landscape Change in SW Alberta using Mountain Legacy Project photography* (Unpublished report). Victoria, BC: University of Victoria.

Hoffman, M.T. & Todd, S. (2010) Using fixed point photography, field surveys, and GIS to monitor environmental change: an example from Riemvasmaak, South Africa. In: Webb, R.H., Boyer, D.E. & Turner, R.M. (Eds.) *Repeat photography: methods and applications in the natural sciences*. Washington, DC: Island Press, pp. 46–56.

Hong, S., Noh, H. & Han, B. (2015) Decoupled deep neural network for semi-supervised semantic segmentation (arXiv:1506.04924). *arXiv*. https://doi.org/10.48550/arXiv.1506.04924

Hung, W.-C., Tsai, Y.-H., Liou, Y.-T., Lin, Y.-Y. & Yang, M.-H. (2018) Adversarial learning for semi-supervised semantic segmentation (arXiv:1802.07934). *arXiv*. https://doi.org/10.48550/arXiv.1802.07934

Jean, F., Albu, A.B., Capson, D., Higgs, E., Fisher, J.T. & Starzomski, B.M. (2015) The mountain habitats segmentation and change detection dataset. *IEEE Winter Conference on Applications of Computer Vision*, **2015**, 603–609. Available from: https://doi.org/10.1109/WACV.2015.86

Keane, R.E., Hessburg, P.F., Landres, P.B. & Swanson, F.J. (2009) The use of historical range and variability (HRV) in landscape management. *Forest Ecology and Management*, **258**(7), 1025–1037. Available from: https://doi.org/10.1016/j.foreco.2009.05.035

Kull, C.A. (2005) Historical landscape repeat photography as a tool for land use change research. *Norsk Geografisk Tidsskrift —Norwegian Journal of Geography*, **59**(4), 253–268. Available from: https://doi.org/10.1080/00291950500375443

Landres, P.B., Morgan, P. & Swanson, F.J. (1999) Overview of the use of natural variability concepts in managing ecological systems. *Ecological Applications*, **9**(4), 1179–1188. Available from: https://doi.org/10.1890/1051-0761(1999)009[1179:OOTUON]2.0.CO;2

MacLaren, P.I.S., Higgs, E. & Zezulka-Mailloux, G. (2005) *Mapper of mountains: M.P. Bridgland in the Canadian Rockies, 1902–1930*, 1st edition. Edmonton, AB: The University of Alberta Press.

Mahdavi, S., Salehi, B., Granger, J., Amani, M., Brisco, B. & Huang, W. (2018) Remote sensing for wetland classification: a comprehensive review. *GIScience & Remote Sensing*, **55**(5), 623–658. Available from: https://doi.org/10.1080/15481603.2017.1419602

Masubelele, M.L., Hoffman, M.T. & Bond, W.J. (2015) A repeat photograph analysis of long-term vegetation change in semi-arid South Africa in response to land use and climate. *Journal of Vegetation Science*, **26**(5), 1013–1023. Available from: https://doi.org/10.1111/jvs.12303

McCaffrey, D.R. & Hopkinson, C. (2017) Assessing fractional cover in the alpine Treeline ecotone using the WSL Monoplotting tool and airborne Lidar. *Canadian Journal of Remote Sensing*, **43**(5), 504–512. Available from: https://doi.org/10.1080/07038992.2017.1384309

McCaffrey, D.R. & Hopkinson, C. (2020) Modeling watershed-scale historic change in the alpine Treeline ecotone using random Forest. *Canadian Journal of Remote Sensing*, **46**(6), 715–732. Available from: https://doi.org/10.1080/07038992.2020.1865792

McClaran, M.P., Browning, D.M. & Huang, C. (2010) Temporal dynamics and spatial variability in desert grassland vegetation. In: Webb, R.H., Boyer, D.E. & Turner, R.M. (Eds.) *Repeat photography: methods and applications in the natural sciences*. Washington, DC: Island Press, p. 145.

Natural Resources Canada. (2021) High Resolution Digital Elevation Model (HRDEM)—CanElevation Series—Product specifications. Available from: https://open.canada.ca/data/en/dataset/0fe65119-e96e-4a57-8bfe-9d9245fba06b

Pal, M. & Mather, P.M. (2005) Support vector machines for classification in remote sensing. *International Journal of Remote Sensing*, **26**(5), 1007–1011. Available from: https://doi.org/10.1080/01431160512331314083

Peterson, A.T., Berthiaume, K., Klett, M. & Munroe, J.S. (2022) Linking repeat photography and remote sensing to assess treeline rise with climate warming: Mount of the Holy Cross, Colorado. *Arctic, Antarctic, and Alpine Research*, **54**(1), 478–487. Available from: https://doi.org/10.1080/15230430.2022.2121245

Rhemtulla, J.M., Hall, R.J., Higgs, E.S. & Macdonald, S.E. (2002) Eighty years of change: vegetation in the montane ecoregion of Jasper National Park, Alberta, Canada. *Canadian Journal of Forest Research*, **32**(11), 2010–2021. Available from: https://doi.org/10.1139/x02-112

Rogers, G.F., Malde, H.E. & Turner, R.M. (1984) *Bibliography of repeat photography for evaluating landscape change*. Salt Lake City: University of Utah Press.

Rose, S. (2020) *An evaluation of deep learning semantic segmentation for landcover classification of oblique ground-based photography* (Unpublished master's thesis). Victoria: University of Victoria.

Roush, W., Munroe, J.S. & Fagre, D.B. (2007) Development of a spatial analysis method using ground-based repeat photography to detect changes in the alpine treeline ecotone, glacier National Park, Montana, USA. *Arctic, Antarctic, and Alpine Research*, **39**(2), 297–308. Available from: https://doi.org/10.1657/1523-0430(2007)39[297:DOASAM]2.0.CO;2

Sanseverino, M.E., Whitney, M.J. & Higgs, E.S. (2016) Exploring landscape change in mountain environments with the mountain legacy online image analysis toolkit. *Mountain Research and Development*, **36**(4), 407–416. Available from: https://doi.org/10.1659/MRD-JOURNAL-D-16-00038.1

Steffen, W., Broadgate, W., Deutsch, L., Gaffney, O. & Ludwig, C. (2015) The trajectory of the Anthropocene: the great acceleration. *The Anthropocene Review*, **2**(1), 81–98. Available from: https://doi.org/10.1177/2053019614564785

Stockdale, C.A., Bozzini, C., Macdonald, S.E. & Higgs, E. (2015) Extracting ecological information from oblique angle terrestrial landscape photographs: performance evaluation of the WSL Monoplotting tool. *Applied Geography*, **63**, 315–325. Available from: https://doi.org/10.1016/j.apgeog.2015.07.012

Trant, A., Higgs, E. & Starzomski, B.M. (2020) A century of high elevation ecosystem change in the Canadian Rocky Mountains. *Scientific Reports*, **10**(1), 9698. Available from: https://doi.org/10.1038/s41598-020-66277-2

Trant, A.J., Starzomski, B.M. & Higgs, E. (2015) A publically available database for studying ecological change in mountain ecosystems. *Frontiers in Ecology and the Environment*, **13**(4), 187. Available from: https://doi.org/10.1890/15.WB.007

Turner, M.G. & Seidl, R. (2023) Novel disturbance regimes and ecological responses. *Annual Review of Ecology, Evolution, and Systematics*, **54**(1), 63–83. Available from: https://doi.org/10.1146/annurev-ecolsys-110421-101120

Walter, T. (2020) Satellite-based augmentation systems (SBASs). In: Morton, Y.J., van Diggelen, F., Spilker, J.J., Jr., Parkinson, B.W., Lo, S. & Gao, G. (Eds.) *Position, navigation, and timing technologies in the 21st century*. Hoboken, NJ: John Wiley & Sons, Ltd., pp. 277–306. Available from: https://doi.org/10.1002/9781119458449.ch13

Webb, R.H., Boyer, D.E. & Turner, R.M. (Eds.). (2010) *Repeat photography: methods and applications in the natural sciences*, 1st edition. Washington, DC: Island Press.

Wulder, M. (1998) Optical remote-sensing techniques for the assessment of forest inventory and biophysical parameters. *Progress in Physical Geography*, **22**(4), 449–476. Available from: https://doi.org/10.1177/030913339802200402

Wulder, M.A., White, J.C., Hay, G.J. & Castilla, G. (2008) Towards automated segmentation of forest inventory polygons on high spatial resolution satellite imagery. *The Forestry Chronicle*, **84**(2), 221–230. Available from: https://cfs.nrcan.gc.ca/publications?id=29414

Zou, Y., Yu, Z., Kumar, B.V.K.V. & Wang, J. (2018) *Domain adaptation for semantic segmentation via class-balanced self-training* (arXiv:1810.07911). *arXiv*. Available from: https://doi.org/10.48550/arXiv.1810.07911

Supporting Information

Additional supporting information may be found online in the Supporting Information section at the end of the article.

Appendix A. List of MLP oblique photographs used for Jasper National Park study area

Appendix B. Oblique photographs and associated land-cover classifications.
Appendix C. Georeferenced landcover classifications.
Appendix D. Maps.